Synergistic effects of in-situ TiB_2 on grain structure and strength of Al–4.5Cu alloys

Shaik Mozammil[1,*], Soumya Ranjan Giri[1], Santanu Pahari[2]

[1] Department of Mechanical Engineering, C.V. Raman Global University Bhubaneswar, 752054, India

[2] Pyrometallurgy and Materials Engineering, CSIR-IMMT Bhubaneswar, 751013, India

*Corresponding author: smozammil@me.iitr.ac.in

Tel. +91 95579 87014

Abstract

In-situ Al–4.5 wt.%Cu–xTiB_2 (x = 3–12 wt.%) composites were synthesized to achieve simultaneous microstructural refinement and mechanical strengthening. Multi-scale characterization reveals that TiB_2 forms uniformly within the Aluminium matrix without parasitic phases, while effectively modifying the morphology and distribution of Al_2Cu precipitates. Increasing TiB_2 content results in pronounced grain refinement, enhanced high-angle grain boundary fraction, and texture randomization, supported by EBSD and TEM analyses. Sub-micron TiB_2 particulates with clean interfaces generate dense dislocation networks and promote heterogeneous nucleation, activating synergistic strengthening via grain refinement, Orowan looping, precipitation hardening, and load transfer. Tensile testing shows a substantial improvement in yield and ultimate strengths, particularly after T6 aging, with optimum strength–ductility balance achieved at 6–9 wt.% TiB_2. These findings demonstrate an efficient pathway for tailoring high-performance Al–Cu matrix composites for lightweight structural applications.

Keywords: In-situ TiB_2, Grain refinement, Mechanical properties, EBSD, TEM

1. Introduction

Al–Cu based aluminium alloys are widely employed in lightweight structural applications due to their high specific strength and excellent precipitation hardening capability; however, their performance is often limited by coarse grain structures and non-uniform Al_2Cu intermetallic networks formed during solidification [1,2]. In-situ synthesized ceramic reinforcements, particularly TiB_2, have emerged as effective microstructural modifiers owing to their thermodynamic stability, crystallographic compatibility with α-Al, and ability to act as potent heterogeneous nucleation sites [3,4]. Recent studies have demonstrated that uniformly dispersed TiB_2 particles can simultaneously promote grain refinement, suppress deleterious intermetallic phases, and enhance load transfer efficiency, resulting in significant improvements in strength without severe loss of ductility [5,6]. Moreover, in heat-treatable Al–Cu systems, TiB_2 reinforcements have been reported to interact synergistically with θ′/θ″ precipitates during aging, leading to multi-scale strengthening effects [7]. Despite these advances, a systematic understanding of the combined influence of TiB_2 content on grain structure evolution, precipitation behavior, texture randomization, and mechanical response in Al–4.5 wt.% Cu alloys remains limited. In this context, the present work reports the microstructural evolution and mechanical performance of in-situ TiB_2 reinforced Al–4.5 wt.% Cu composites, highlighting the optimal reinforcement range for achieving a superior strength–ductility balance.

2. Experimental procedure and characterization

Al-4.5 wt.%Cu-xTiB_2 (x = 3, 6, 9 and 12 wt.%) in-situ composites were fabricated by controlled stir-assisted salt reaction route. Aluminium and copper in the form of commercially pure were melted at 780 °C in an electric furnace to obtain Al-4.5wt.%Cu melt. In-situ TiB_2 was synthesized by addition of calculated amounts of K_2TiF_6 and KBF_4 salts into the molten alloy with cryolite (Na_3AlF_6, 10 g) added for moderating the reaction kinetics and to ensure the compositional balance. Stirring was performed with a steel impeller under optimized

conditions of impeller position, size and rotational speed to ensure uniform particle dispersion and low porosity. The exothermic reaction between the melt and salts produced TiB_2 particles along with $KAlF_4$ slag, which was readily separated from the melt. Reaction holding times were varied between 30 and 75 min at 780 °C to control TiB_2 yield, while maintaining a Ti:B ratio of 2.2:1 to suppress the formation of brittle Al_3Ti and AlB_2 phases. The processing temperature was restricted below 820 °C to avoid KBF_4 dissociation and boron loss. Prior to casting, the melt was degassed using C_2Cl_6 and poured into a metallic mould. The resulting exothermic reaction between molten metal and salts is given below.

$$Al - Cu + K_2TiF_6 + KBF_4 \rightarrow Al + TiB_2 + Al_2Cu + KAlF_4 + Heat$$

Microstructural characterization was performed on metallographically prepared specimens etched with Keller's reagent. Nanoscale features and matrix–reinforcement interfaces were investigated using high-resolution transmission electron microscopy on electron-transparent foils prepared by twin-jet electropolishing. Tensile properties were evaluated using ASTM E8 specimens on a universal testing machine to assess strength and deformation behaviour. For precipitation strengthening, selected samples were subjected to a T6 heat-treatment cycle consisting of solution treatment at 540 °C for 2 h, water quenching, and artificial ageing at 170 °C for durations ranging from 5 to 25 h, followed by air cooling.

3. Results and discussion

Optical and SEM micrographs of the unreinforced alloy (Fig. 1(a) & Fig. 1(f)) show the coarse α-Al matrix with discontinuous Al_2Cu intermetallic preferentially segregated along the grain boundaries, suggesting non-uniform solidification. With the addition of TiB_2 (Fig. 1(b-e) & Fig.1(g-j)), there is the appearance of a progressive refinement and homogenization of the microstructure. At 3 wt.% TiB_2, finely and uniformly dispersed TiB_2 particles act as good heterogeneous nucleation sites resulting in a significant grain refinement and suppression of

coarse Al_2Cu networks. Increasing the reinforcement content to 6 and 9 wt.% improves the uniformity of the microstructure more obviously, and TiB_2 can be seen as discrete and well distributed particles in the matrix, indicating the effective in-situ formation and good interfacial bonding. At 12 wt.% TiB_2, the use of a higher particle density is evident, in combination with local clustering, but the Al_2Cu phase is nevertheless refined and uniformly distributed in the matrix. SEM-EDS analysis validates the presence of Al, Cu, Ti, and B which confirms the formation of Al_2Cu and TiB_2 phases with no undesirable reaction products while the gradual increase in Ti and B contents with reinforcement level is in accordance with the compositional design.

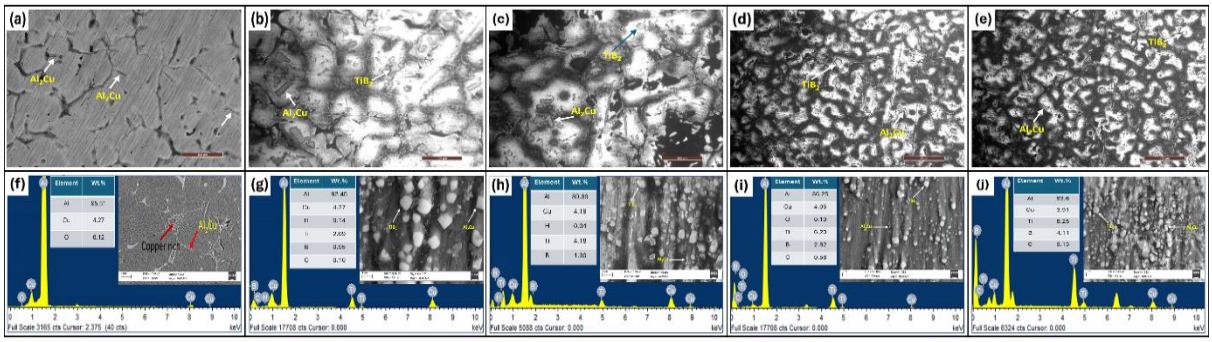

Fig. 1. Optical (a–e) and SEM (f–j) micrographs of Al–4.5 wt.% Cu alloy and Al–4.5 wt.% Cu–xTiB_2 composites (x = 3, 6, 9, 12 wt.%), illustrating microstructural refinement, Al_2Cu distribution, and in-situ TiB_2 dispersion with increasing reinforcement.

XRD patterns of the base alloy and composites (Fig. 2(a)) show dominant α-Al peaks in all samples along with characteristic reflections of the Al_2Cu phase. With increasing TiB_2 content, distinct TiB_2 peaks appear and intensify, confirming successful in-situ synthesis and uniform incorporation of the ceramic reinforcement. TEM analysis of the Al-4.5 wt.% Cu-12 wt.% TiB_2 composite (Fig. 2(b)) indicates that the submicron TiB_2 particles are well dispersed and have clean and well-bonded interfaces. The evenness of the spatial distribution of Al, Cu, Ti, and B is also confirmed by elemental mapping (Fig. 2(c)) without agglomeration. The HRTEM image (Fig. 2(d)) demonstrates that there are nanograins around TiB_2 particles with an interplanar distance of approximately 3.24 A° which is an indication of the refinement of the grains formed by heterogeneous nucleation. Also, a higher concentration of dislocations and dislocation loops

around TiB_2 particles are seen (Fig. 2(e)) due to dislocation caused by incompatibility of thermal expansion between the reinforcement and the matrix, thus causes dislocation strengthening.

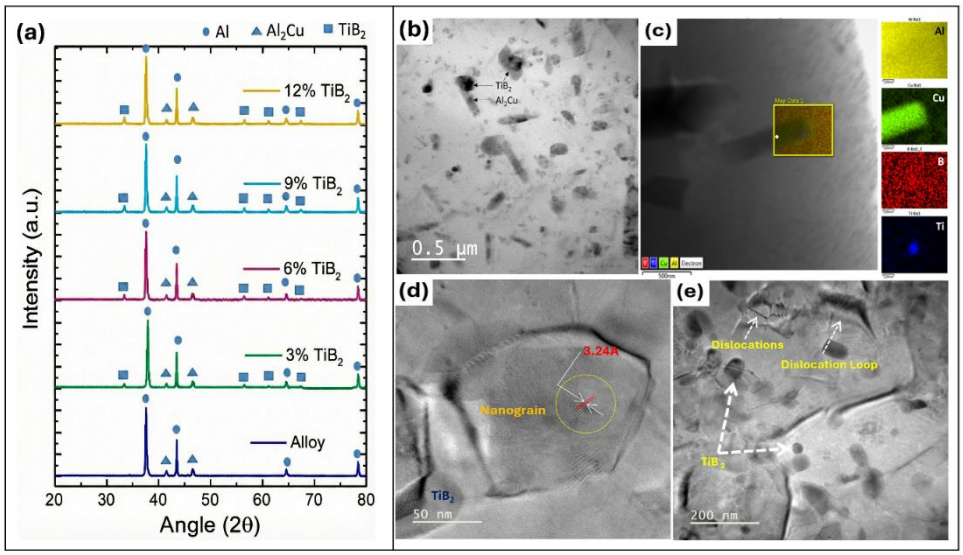

Fig.2. (a) XRD patterns of Al–4.5 wt.% Cu and Al–4.5 wt.% Cu–xTiB_2 composites (x = 3–12 wt.%); (b) TEM micrograph of Al–4.5 wt.% Cu–12 wt.% TiB_2 composite; (c) elemental maps of Al, Cu, Ti, and B; (d) HRTEM image showing lattice fringes (~3.24 Å); (e) dislocations and dislocation loops near TiB_2 particles.

EBSD analysis of the Al–4.5wt.% Cu–12 wt.% TiB_2 composite (Fig.3(a–f)) further substantiates these observations. The inverse pole figure map (Fig.3(a)) reveals a fine, equiaxed grain structure with random crystallographic orientation, confirming effective grain refinement induced by TiB_2 particulates. The corresponding phase map (Fig.3(b)) shows a uniform distribution of TiB_2 along grain boundaries and within the matrix, indicating strong interfacial bonding and effective particle pinning during solidification. The grain size distribution (Fig. 3(c)) exhibits a narrow unimodal peak in the sub-micron regime, reflecting suppressed grain coarsening due to Zener pinning. The misorientation angle distribution (Fig.3(d)) is dominated by high angle grain boundaries (>15°), enhancing grain boundary strengthening. Pole figures of TiB_2 (Fig.3(e)) display weak texture intensity, suggesting random orientation of reinforcement particles, while aluminium pole figures (Fig.3(f)) also exhibit diffuse and low

intensity texture, confirming that TiB_2 effectively disrupts preferred orientation development and promotes near isotropic crystallographic behaviour.

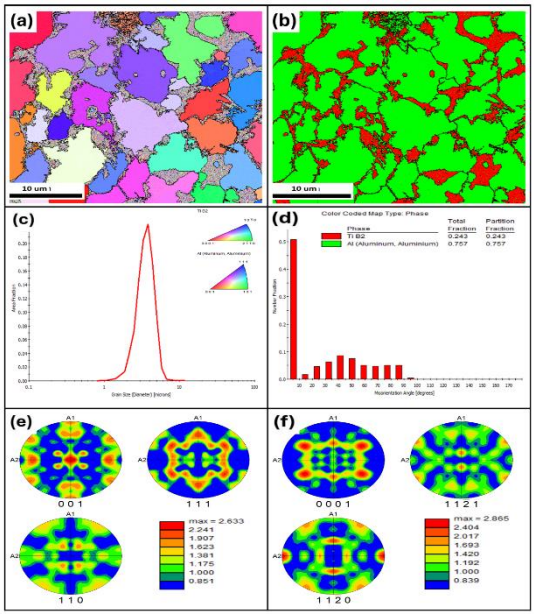

.**Fig. 3.** EBSD analysis of Al–4.5 wt.% Cu–12 wt.% TiB_2 composite: (a) IPF orientation map, (b) phase map, (c) grain size distribution, (d) grain boundary misorientation distribution, (e) TiB_2 pole figures, and (f) aluminium pole figures showing weak texture intensity.

The tensile fracture morphologies of the base alloy or composites (Fig.4(a-e)) demonstrate that there is a distinct change in fracture behavior with respect to increasing TiB_2 content. The alloy that has not been reinforced has large equiaxed dimples and smooth tear ridges similar to those typical of ductile fracture that is controlled by the micro void coalescence. In TiB_2 3 wt.% fracture surface exhibits refined dimples and localized particle-matrix debonding which means enhanced load transfer that is accompanied by initial stress concentrations sites. However, at 6 wt.% TiB_2, uniformly ground fine dimples and well-strong particles indicates an optimum ratio between strength and ductility. Additional increase to 9 and 12 wt.% TiB_2 would lead to finer dimples sprinkled between cleavage-like facets and fracture of the particles, which indicate greater brittleness because of limited plastic deformation and concentrated particle clusters.

The tensile properties in the as-cast and T6 peak-aged conditions (Fig.4(f, g)) indicate that the tensile properties, yield strength and ultimate tensile strength, increase strictly with the increase

of TiB_2 content in the as-cast, and the elongation increases at lower reinforcement and decreases at higher contents. The strength is greatly increased by T6 heat treatment in all compositions and the greatest increase was noted in the 9-12 wt.% TiB_2 composites. This strengthening arises from the synergistic interaction between finely dispersed θ′/θ″ precipitates formed during aging and the thermally stable TiB_2 particles, which collectively impede dislocation motion. Although peak aging leads to a marginal reduction in elongation, composites with intermediate TiB_2 content retain appreciable ductility, consistent with the observed fine dimpled fracture features.

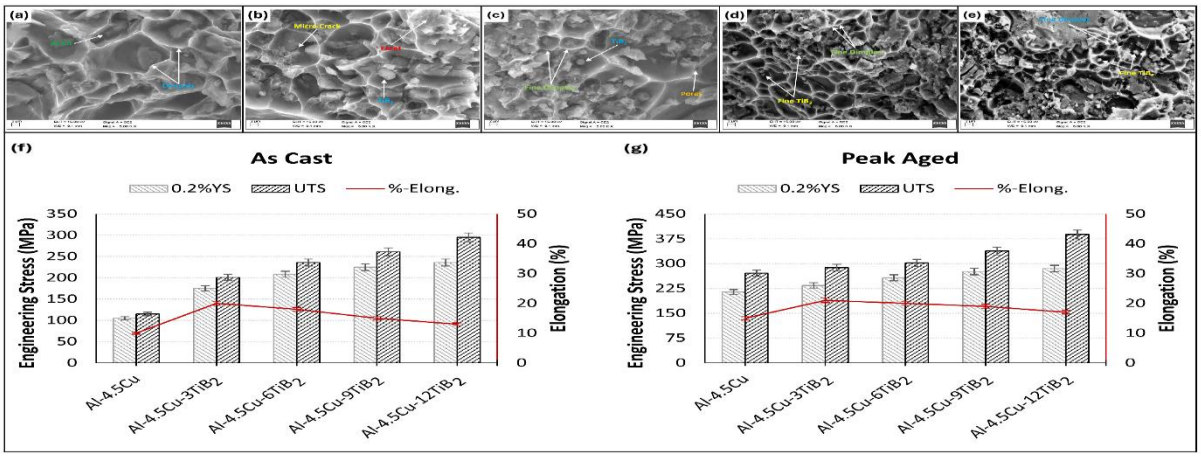

Fig. 4. SEM tensile fracture surfaces of (a) Al–4.5 wt.% Cu and Al–4.5 wt.% Cu–xTiB□ composites with (b) 3, (c) 6, (d) 9, and (e) 12 wt.% TiB□; corresponding tensile properties showing 0.2% YS, UTS, and elongation in (f) as-cast and (g) T6 peak-aged conditions.

Overall, in-situ synthesized TiB_2 simultaneously promotes grain refinement, precipitation strengthening, dislocation strengthening, and effective load transfer, resulting in a superior strength–ductility synergy. Among the investigated compositions, Al–4.5 wt.% Cu composites reinforced with 6–9 wt.% TiB_2 exhibit the most favourable combination of high strength and acceptable ductility, making them promising candidates for lightweight structural applications.

4. Conclusion

In-situ Al–4.5wt.%Cu–xTiB_2 (x = 3–12 wt.%) composites were successfully synthesized, exhibiting uniform TiB_2 formation and refined Al_2Cu precipitates without deleterious phases.

Increasing TiB_2 content promotes strong grain refinement through heterogeneous nucleation and Zener pinning, resulting in fine equiaxed grains, a high fraction of high-angle grain boundaries, and weak texture. Sub-micron TiB_2 particles with clean interfaces generate dense dislocation networks and stabilize θ′/θ″ precipitates during T6 aging, enabling concurrent grain boundary, Orowan, precipitation, dislocation, and load-transfer strengthening. Tensile properties improve markedly with TiB_2 addition, with further enhancement after T6 treatment, while fracture behavior evolves from ductile to mixed ductile–brittle at higher contents. An optimal strength–ductility balance is achieved at 6–9 wt.% TiB_2, demonstrating the effectiveness of controlled in-situ TiB_2 reinforcement for high-performance Al–Cu structural alloys.

References

[1] Y. Zhang, A. Wang, T. Liang, J. Zhang, Z. Mao, D. Yang, J. Xie, H. Zhang, Mater. Charact. 212 (2024) 114009.

[2] Y. Zhou, M. Lin, C. Liu, L. Wang, H. Chen, C. Dan, S. Ma, Z. Chen, H. Wang, J. Alloys Compd. 913 (2022) 165172.

[3] T. Liu, W. Huang, Y. Hu, J. Luo, J. Wu, L. Zhu, Mater. Today Commun. 42 (2025).

[4] M. Dammak, A. Bouhamed, H. Jrad, F. Dammak, Mater. Today Commun. 38 (2024) 107741.

[5] X. Wen, B. Chen, Z. Chen, X. Lin, H. Yang, N. Kang, Q. Wang, W. Wang, W. Huang, Mater. Sci. Eng. A. 847 (2022) 143290.

[6] Y. He, M. Taheri, Y. Zou, A. Lashkari, K. Shirvani, K. Beirami, A.P. Moghaddam, Mater. Lett. 365 (2024) 136449.

[7] X. Yang, B. Jiang, Y. Wang, H. Xu, M. Hu, Y. Guo,Mater. Lett. 381 (2025).